J. Fluid Mech. (1971), *vol.* 45, *part* 4, *pp.* 805–829
Printed in Great Britain

A numerical study of the Bénard cell

By ANDRÉ CABELLI AND G. DE VAHL DAVIS
The University of New South Wales, Kensington, Australia

(Received 20 April 1970)

When a layer of liquid is heated from below at a rate which exceeds a certain critical value, a two- or three-dimensional motion is generated. This motion arises from the action of buoyancy and surface tension forces, the latter being due to variations in the temperature of the liquid surface.

The two-dimensional form of the flow has been studied by a numerical method. It consists of a series of rolls, rotating alternately clockwise and anticlockwise, which are shown to be symmetrical about the dividing streamlines. As well as a detailed description of the motion and temperature of the liquid, and of the effects on these characteristics of variations in the Rayleigh, Marangoni, Prandtl and Biot numbers, a study has been made of the conditions under which the motion first starts, the wavelength of the rolls and the rate of heat transfer across the liquid layer.

Introduction

Motion in heated liquid layers had been observed (Thompson 1855) approximately fifty years before Bénard (1900*a*, *b*) began a systematic study of the phenomenon which now bears his name. Steady-state patterns may be observed when, under certain conditions, a vertical temperature gradient is applied to a thin liquid layer. Density stratification was first thought to be the driving force, and this led to studies of natural convection in fluid layers. More recently, however, it has been realized that, for liquids with free surfaces, variations in temperature could cause surface tension gradients which may be at least as significant as the buoyancy forces. The onset of instability was first studied by Pearson (1958), who attributed the cellular motion observed by Bénard to the action of surface tension alone, and he made a small disturbance analysis for a liquid layer, the lower surface of which was in contact with a rigid boundary while the free upper surface remained plane.

Two boundary conditions were imposed on the lower surface, namely, insulating and conducting. For both cases he found a critical value of the Marangoni number below which the disturbances would decay and the fluid remain stable.

Later investigations, including those of Nield (1964), Scriven & Sternling (1964) and Smith (1966), have refined Pearson's analysis to include the effects of buoyancy and surface deformation.

The aim of this investigation has been to study the detailed behaviour of the motion when surface tension and buoyancy are coupled. Our model, similar to Nield's, is that of a two-dimensional layer of liquid, resting on a rigid surface,

the temperature of which is maintained constant and higher than that of the fluid above the free surface. Heat is transferred by conduction and (if motion occurs) by convection to the upper liquid surface. It is then transferred to the surrounding fluid by convection at a rate determined by a prescribed surface heat transfer coefficient. The temperature of this fluid 'at infinity' is assumed constant. If the liquid is in motion, the temperature of its surface will not be constant, and as a result there will be a variation of surface tension which will contribute to the motion.

In the analysis of the motion, the following assumptions were made:

(i) Viscous dissipation is negligible and internal energy generation absent.
(ii) The Boussinesq approximations are valid.
(iii) The free surface remains undeformed.
(iv) Evaporation from the free surface is negligible.
(v) The fluid above the free surface exerts no tangential force on the surface.

Derivation of equations

The equations describing the motion are those expressing conservation of mass, momentum and energy, which may be written for the above assumptions as:

$$\frac{\partial u'}{\partial x'} + \frac{\partial v'}{\partial y'} = 0, \tag{1a}$$

$$\frac{Du'}{Dt'} = -\frac{1}{\rho_0}\frac{\partial p'}{\partial x'} + \{1 - \beta(\theta' - \theta_0')\}g + \nu\nabla'^2 u', \tag{1b}$$

$$\frac{Dv'}{Dt'} = -\frac{1}{\rho_0}\frac{\partial p'}{\partial y'} + \nu\nabla'^2 v', \tag{1c}$$

$$\frac{D\theta'}{Dt'} = \frac{k}{\rho_0 C_p}\nabla'^2\theta'. \tag{1d}$$

The geometric configuration and co-ordinates are shown in figure 1. u' and v' are the velocity components in the x' (vertically downwards) and y' (horizontal) directions; ρ, β, ν, k and C_p denote respectively the density, volumetric expansion coefficient, kinematic viscosity, thermal conductivity and specific heat of the liquid; p' and θ' are the pressure and temperature of the liquid; t' denotes time. Primes denote dimensional quantities, and the subscript 0 indicates some reference state, say that of the surrounding fluid.

We introduce variables P' and T' to denote departures of pressure and temperature from the hydrostatic (pure conduction) situation, through the equations,

$$p' = P' + p_s' \quad \text{and} \quad \theta' = T' + \theta_s', \tag{2a,b}$$

where p_s' and θ_s' are the pressure and temperature respectively in the absence of motion. The momentum equations (1*b*, *c*) are now

$$\frac{Du'}{Dt'} = -\frac{1}{\rho_0}\frac{\partial P'}{\partial x'} - g\beta T' + \nu\nabla'^2 u', \tag{3a}$$

$$\frac{Dv'}{Dt'} = -\frac{1}{\rho_0}\frac{\partial P'}{\partial y'} + \nu\nabla'^2 v'. \tag{3b}$$

Combining these by cross-differentiation to eliminate pressure, we obtain

$$\frac{D\zeta'}{Dt'} = g\beta\frac{\partial T'}{\partial y'} + \nu\nabla'^2\zeta', \tag{4}$$

where the vorticity ζ' is $\dfrac{\partial v'}{\partial x'} - \dfrac{\partial u'}{\partial y'}$.

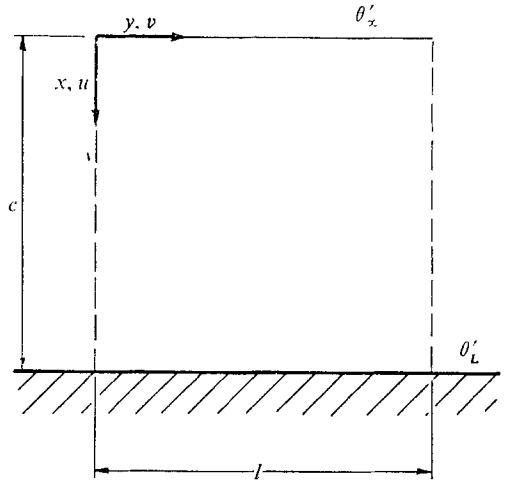

FIGURE 1. Co-ordinate system.

Under conditions of pure conduction, the temperature distribution $\theta'_s(x)$ is linear; the energy equation (1*d*) thus becomes

$$\frac{DT'}{Dt'} + u'\frac{\partial\theta'_s}{\partial x'} = \frac{k}{\rho_0 C_p}\nabla'^2 T'. \tag{5}$$

We define a stream function ψ' by

$$u' = \frac{\partial\psi'}{\partial y'}, \quad v' = -\frac{\partial\psi'}{\partial x'}; \tag{6a, b}$$

and it follows that

$$\zeta' = -\nabla'^2\psi'. \tag{7}$$

When introducing dimensionless quantities, we see that the surface temperature θ'_u is not useful, since it varies, and is determined by the motion of the liquid and by convection to the fluid over the liquid. This temperature is given by

$$k\frac{\partial\theta'}{\partial x'} = h_a(\theta'_u - \theta'_\infty), \tag{8}$$

where h_a is the surface convection coefficient, and θ'_∞ is the fluid temperature far above the surface. The dimensionless temperature θ is defined instead as

$$\theta = \frac{\theta' - \theta'_\infty}{\theta'_L - \theta'_\infty},$$

where θ'_L is the lower surface temperature. The remaining dimensionless quantities are

$$x = x'/c, \quad y = y'/c, \quad t = t'\nu/c^2, \quad \text{and} \quad \psi = \psi'/\nu,$$

where c is the depth of the liquid layer.

The equations then become

$$\frac{D\zeta}{Dt} = Gr\frac{\partial T}{\partial y} + \nabla^2\zeta, \tag{9a}$$

$$\zeta = -\nabla^2\psi, \tag{9b}$$

$$\frac{DT}{Dt} + u\frac{Bi}{1+Bi} = \frac{1}{Pr}\nabla^2 T, \tag{9c}$$

where

Gr = Grashof number = $g\beta c^3(\theta'_L - \theta'_\infty)/\nu^2$,

Pr = Prandtl number = $\rho C_p \nu/k$,

Bi = Biot number = $h_a c/k$.

Boundary conditions

Following Pearson (1958), and assuming that normal stresses vary negligibly along the free surface, a force balance shows that

$$\frac{\partial^2 u}{\partial x^2} = -\frac{Ma}{Pr}\frac{\partial^2 T}{\partial y^2}, \tag{10a}$$

which may be written in terms of vorticity as

$$\frac{\partial \zeta}{\partial y} = \frac{Ma}{Pr}\frac{\partial^2 T}{\partial y^2}, \tag{10b}$$

where Ma = Marangoni number = $[\gamma C_p(\theta'_L - \theta'_\infty)c]/\nu k$, and γ is the temperature coefficient of surface tension (σ):

$$\sigma = \sigma_0 - \gamma(\theta' - \theta'_0).$$

The thermal boundary condition at the free surface (8) may be written

$$\partial\theta/\partial x = Bi.\theta_u, \tag{11a}$$

or, in terms of the convection temperature,

$$\partial T/\partial x = Bi.T_u, \tag{11b}$$

where the subscript u denotes the free upper surface. The free surface vertical velocity u is zero as a result of the assumption of a non-deforming surface, and $\psi = 0$. The lower surface is isothermal and rigid; hence, $T = u = v = \psi = 0$.

Conditions at the side boundaries of the solution region are not clear. Anticipating that the motion in an infinitely wide layer will take the form of periodic rolls, we are interested in determining the periodicity (i.e. the roll wavelength in terms of the depth of the layer) and cannot specify this *a priori*. Moreover, we cannot be sure that the dividing streamline between adjacent rolls will be vertical.

Accordingly, we are first of all forced to assume a value for the roll wavelength in order to fix the size of the solution region. Following Malkus (1954*a*, *b*), the *preferred* wavelength for given parameters (*Gr*, *Pr*, *Ma* and *Bi*) will be taken as that which maximizes the rate of heat transfer.

With the roll size fixed, we still have two possible lateral boundary conditions. The more general, and more obvious, alternative is to examine a pair of rolls and invoke the periodic nature of the flow. As discussed below, the results of this approach suggested that in fact the dividing streamlines *were* vertical and formed lines of symmetry between adjacent rolls. Most solutions were therefore obtained with this latter condition, which has the computational attraction that the storage requirement and computing time are virtually halved.

The Nusselt number (*Nu*), or dimensionless rate of heat transfer, is a property of practical interest. Since the velocity at the lower surface is zero, *Nu* could be evaluated from the temperature gradient there. However, this requires the use of inaccurate one-sided finite difference approximations. Additionally, therefore, the combined conduction and convection heat transfer rates were horizontally averaged and computed as a function of depth below the surface. It can be readily shown that

$$Nu = \frac{1}{L}\left[\int_0^L \frac{\partial\theta}{\partial x}\,dy - Pr\int_0^L u\theta\,dy\right], \tag{12a}$$

or, if calculated at the upper or lower boundaries

$$Nu = \frac{Bi}{1+Bi} + \frac{1}{L}\int_0^L \frac{\partial T}{\partial x}\,dy, \tag{12b}$$

where L is the dimensionless width. *Nu* here is defined as the heat flux per unit temperature difference between the lower surface and the fluid far above the free surface. Later, a Nusselt number based upon the average temperature difference across the liquid layer will be introduced.

Method of solution

The equations and boundary conditions were approximated using finite differences and solved at the nodes of a rectangular grid superimposed on the domain. The vorticity and energy transport equations were solved using the alternating direction implicit scheme outlined by Brian (1961), which consists essentially of breaking the time step into two equal parts and approximating the equations implicitly in one direction and explicitly in the other for the first half time step, the procedure then being reversed for the second half time step. Two intermediate values of the time dependent variable (T or ζ) are obtained. An explicit relationship is then derived which satisfies the equation and is used to eliminate the second intermediate value by substitution. (This method involves fewer operations than the more conventional A.D.I. scheme; it also possesses the advantage of numerical stability when applied to three-dimensional problems, which are also under investigation.) The problem is thus reduced to two consecutive solutions of sets of tri-diagonal equations for each of the energy and vorticity equations.

Since the boundary conditions for vorticity are unknown (except at a stress-free surface, where $\zeta_b = 0$), ζ_b was obtained from the stream function field, or, at the free surface, was forced through the appropriate boundary condition. Hence, the vorticity equation was solved only for the interior points of the domain. The boundary vorticity was estimated after each half iteration, thus reducing the time lag and improving the accuracy of the method. In addition to speed convergence, variable time steps were used.

The elliptic equation (9*b*) for ψ was solved by point over-relaxation, the over-relaxation factor being empirically varied to minimize the number of iterations required.

Initial conditions were obtained either by imposing a random temperature fluctuation to the whole field for the first time step with the fluid initially at rest, or by starting from a previously converged solution with different parameters. The latter often proved to be more economical in terms of computer time, provided the change in parameters was not too drastic and only the final steady state was required. Certain questions arise, however, regarding the mode of motion as a result of this technique; these are discussed below.

Except where otherwise stated, the results presented here were obtained using a vertical mesh size of $\frac{1}{20}$ of the layer depth and a horizontal mesh size of $\frac{1}{20}$ of the roll width. (As discussed below, the roll width is a variable of the solution, but the number of mesh points was independent of its value.) The solutions were obtained on an IBM 360/50 digital computer.

Description of the flow

The majority of the results have been obtained for the case of symmetric lateral boundary conditions. It is convenient, first, to describe the principal features of the flow thus obtained, and then return to a consideration of whether such boundary conditions are, in fact, valid. (Readers are assured that we think they are.)

The motion was constrained to lie in two dimensions and, as anticipated, established itself in the form of rolls. With symmetric boundary conditions it was only necessary to study one roll. The direction of rotation of the roll was not predetermined and depended upon the initial conditions. In the results described here, for single rolls, the rotation is always anti-clockwise.

Four cases are used to illustrate the general features of the flow and the parameters for each of these are shown in table 1.

Figures 2(*a*)–(*d*) show streamline and isotherm distributions† for the different combinations of Grashof and Marangoni numbers, with the Biot and Prandtl numbers held constant. The values of Bi and Pr are not particularly representative of practical situations. ($Bi = 100$ is high for natural convection, but might be appropriate when significant evaporation occurs, although mass transfer has

† In these and subsequent contour plots, the figures adjacent to the contours indicate the values of the plotted function as a percentage of the total range of values for the respective plots.

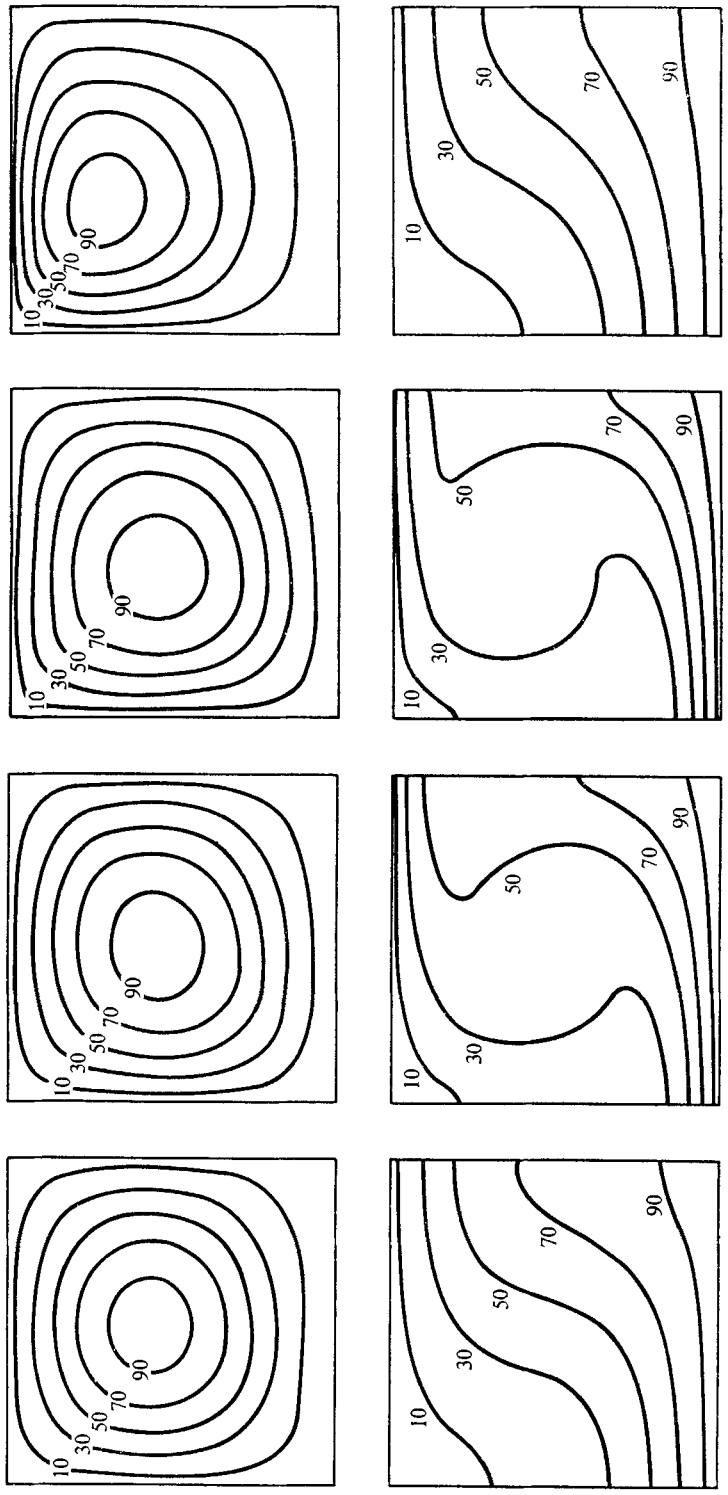

FIGURE 2. Streamline and isotherm contours (*a*) for case *A*: $\psi'_{\max} = 3{\cdot}32$, $\psi'_{\min} = 0$, $\theta_{\max} = 1$, $\theta_{\min} = 0{\cdot}33 \times 10^{-2}$; (*b*) for case *B*: 12·24, 0, 1, $0{\cdot}55 \times 10^{-2}$; (*c*) for case *C*: 13·77, 0, 1, $0{\cdot}58 \times 10^{-2}$; (*d*) for case *D*: 2·70, 0, 1, $0{\cdot}22 \times 10^{-2}$.

not been considered in the solution; $Pr = 1$ is, of course, somewhat low for a liquid.) Nevertheless, the results display the characteristic features of the effects of variation of Gr and Ma. The aspect ratio α of the roll (i.e roll width divided by layer depth) is at its optimum value for each situation. The determination of α_{opt} is discussed below.

It will be observed, first, that the fluid temperature decreases as it moves over the surface. As far as is known to the authors, a decrease in temperature always results in an increase in surface tension (a situation which has been implied in the definition of γ, in order to yield positive values of Ma). It can therefore be anticipated, and it was found, that an increase in Ma results in an intensification of the motion.

	Case *A*	Case *B*	Case *C*	Case *D*
Gr	1,750	10,000	10,000	100
Pr	1	1	1	1
Bi	100	100	100	100
Ma	0	0	5,000	5,000
α_{opt}	1·15	0·97	0·85	0·94

TABLE 1. The parameters of the solutions used to display the principal features of the flow

Without surface tension, the roll centre was always near the centre of the domain. An increase in Marangoni number, however, caused the roll centre to shift upward and in the direction of the free surface motion. This effect has also been observed experimentally: figure 23 of the paper by Berg, Acrivos & Boudart (1966) shows two-dimensional rolls in which "cold fluid flows down in a relatively narrow region near the roll partition, while warm liquid rises over a wider, less distinct region". The shift of the roll centre was more pronounced at lower Grashof numbers as can be seen in figure 2(*d*). In the extreme case of low buoyant forces and high surface tension, a flow developed which was similar to that induced by sliding a rigid surface across an enclosed cavity, as studied by Greenspan (1968).

Figures 3(*a*)–(*l*) show the corresponding contours of horizontal and vertical velocities and the vorticity distribution throughout the field. The highest horizontal velocity always occurred at the free surface while the highest vertical velocity was always found at the vertical boundaries. For the cases shown so far, the warm (upward) current was slower than the cooler (downward) current, and this effect was accentuated when surface tension was present. As a measure of this phenomenon, the ratio of the maximum vertical velocities was calculated (maximum downward/maximum upward), and the values obtained were 1·067, 1·144, 1·351 and 1·968 for cases *A* to *D*, respectively. This condition was found to be a function of the Prandtl number and is discussed later.

The region of highest vorticity for a stress free surface ($Ma = 0$) was the rigid lower boundary. As the Marangoni number was increased, however, the upper surface was stressed and velocity gradients imposed, thus leading to a new source of vorticity the strength of which, for the cases shown, exceeded that of

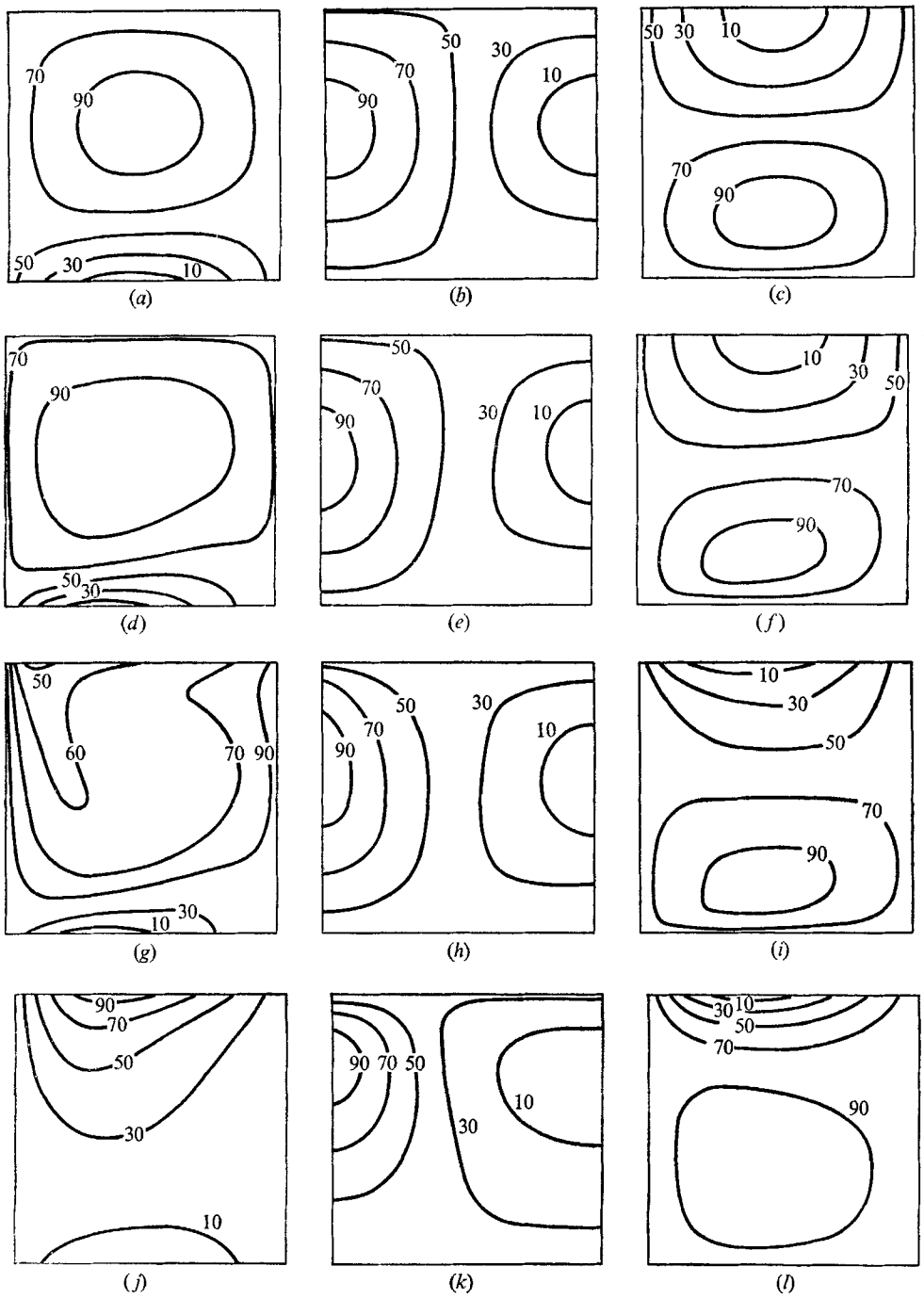

FIGURE 3. Vorticity, vertical and horizontal velocity contours for case A:

(a) $\zeta_{\max} = 0{\cdot}65 \times 10^2$, $\zeta_{\min} = -0{\cdot}88 \times 10^2$,
(b) $u_{\max} = 0{\cdot}95 \times 10$, $u_{\min} = -0{\cdot}89 \times 10$,
(c) $v_{\max} = 0{\cdot}90 \times 10$, $v_{\min} = -0{\cdot}12 \times 10$;

for case B: (d) $0{\cdot}23 \times 10^3$, $-0{\cdot}49 \times 10^3$, (e) $0{\cdot}49 \times 10^2$, $-0{\cdot}43 \times 10^2$, (f) $0{\cdot}36 \times 10^2$, $-0{\cdot}46 \times 10^2$;
for case C: (g) $0{\cdot}68 \times 10^3$, $-0{\cdot}59 \times 10^3$, (h) $0{\cdot}70 \times 10^2$, $-0{\cdot}51 \times 10^2$, (i) $0{\cdot}41 \times 10^2$, $-0{\cdot}72 \times 10^2$;
for case D: (j) $0{\cdot}19 \times 10^3$, $-0{\cdot}37 \times 10^2$, (k) $0{\cdot}13 \times 10^2$, $-0{\cdot}66 \times 10$, (l) $0{\cdot}53 \times 10$, $-0{\cdot}25 \times 10$.

the lower boundary. A central core of nearly constant vorticity existed at low Ma, which might justify the boundary-layer approximations taken by Pillow (1952) and by Robinson (1967). As Ma increased, however, this feature disappeared.

More detailed information on the stream function and velocity distribution for the same four cases can be seen on figures 4–7.

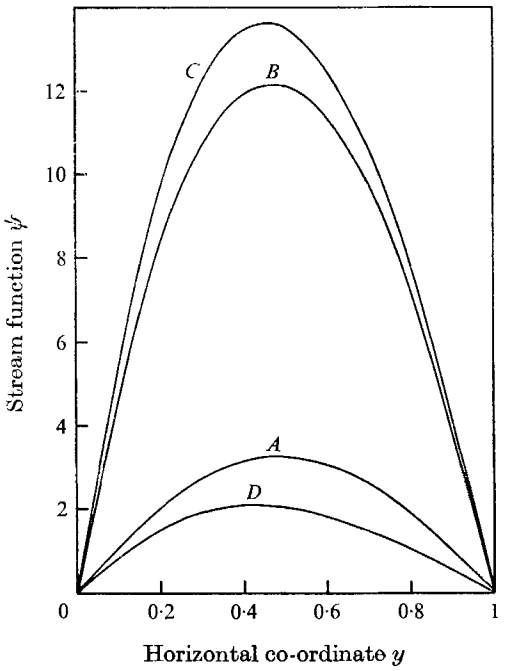

FIGURE 4. The distribution of stream function across the mid-height of the layer for cases *A–D*.

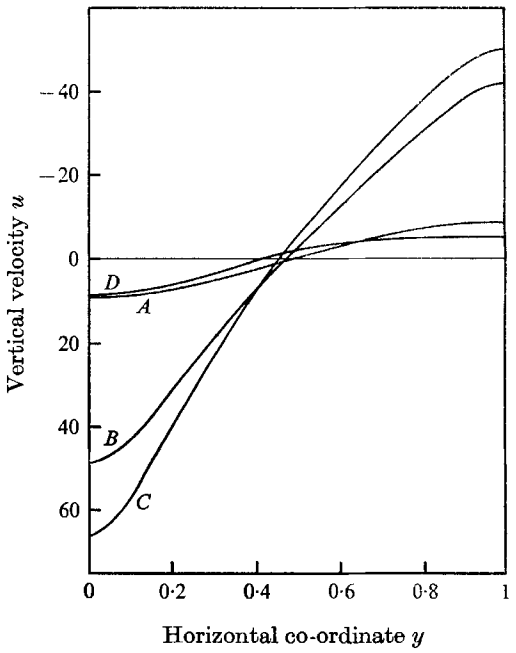

FIGURE 5. The distribution of vertical velocity across the mid-height of the layer for cases *A–D*.

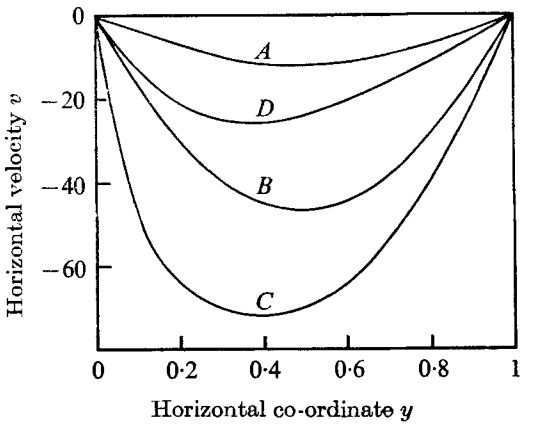

FIGURE 6. The distribution of horizontal velocity across the surface of the layer for cases *A–D*.

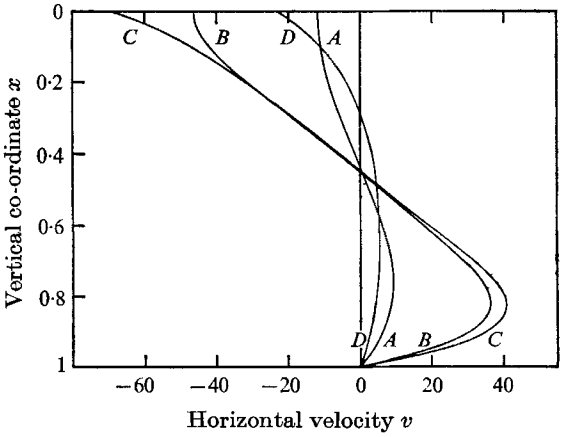

FIGURE 7. The distribution of the horizontal velocity along the vertical centre-line of the solution region for cases *A–D*.

Figures 8–12 show the temperature distribution at selected horizontal and vertical cross-sections. As the Marangoni number was increased, the fluid reached the free surface at a higher mean temperature and the overall heat transfer increased. For the slower convective motion (low Gr and/or Ma), the horizontally averaged temperature gradient was low and fairly uniform throughout the depth of the domain, as can be seen from figures 10–12. As the strength of the motion increased, however, these gradients became steeper near the horizontal boundaries and, at the centre of the domain, zero or even reversed gradients could form, with warmer fluid lying above cooler fluid. The mean vertical temperature gradient near the upper boundary was generally lower than that near the rigid boundary, which confirms the observation of Di Federico & Foraboshi (1966). Right at the horizontal boundaries, however, these gradients were found to be identical (within the limits of numerical accuracy). This is as it should be, since there the only mode of heat transfer is by conduction at a rate given by the vertical temperature gradient. The temperature distribution along the centre-lines of the upward and downward currents are also shown. The upward, hotter current exhibited its highest gradient at the upper boundary, while the opposite effect occurred with the downward moving fluid.

Optimum aspect ratio

In the numerical simulation of the motion, a solution of the equations may be found for any roll wavelength by selecting the aspect ratio α (the ratio of width of the solution domain to its depth) for the particular solution. It is expected, however, that whereas solutions for any α are theoretically valid, one of them will be preferred in nature. The criterion which is generally used to specify the preferred wavelength is that proposed by Malkus (1954*a*, *b*): the fluid will tend to flow in a manner which maximizes the rate of heat transfer. This was confirmed in the proof given by Schlüter *et al.* (1965), but has been questioned by Foster (1969), who gave an example for which, at a particular value of Gr, white noise disturbances grew into a two-roll solution with a resulting Nusselt number 5 % lower than that for an equivalent one-roll solution with identical parameters. He concluded that Malkus's criterion "is not valid at low Rayleigh numbers for two-dimensional flow", and that "there are under certain conditions more than one metastable solution which can develop depending upon the initial conditions". However, the value of α used by Foster in this test was 1·8; this was not the optimum value, which was about 1·4 (i.e. it was not the α yielding the maximum Nusselt number). If the Malkus criterion is correct, the motion could not develop into either one or two rolls in a width of 1·8; it would develop into a roll of width 1·4. Furthermore, Foster found, as we do (see figure 20 below), that a multi-roll solution computed at a multiple of α_{opt} yielded the same Nusselt number as a single-roll solution computed at α_{opt}. The point is that solutions computed away from α_{opt} are physically meaningless, and cannot be used to predict the behaviour of a real fluid. (These remarks, of course, do not apply to a situation with rigid side walls.) We believe that numerical results cannot be used to prove or disprove

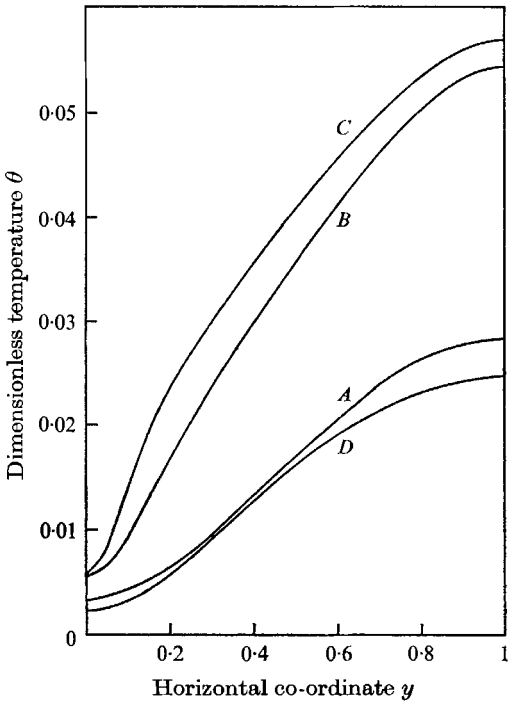

FIGURE 8. The distribution of temperature across the surface for cases *A–D*.

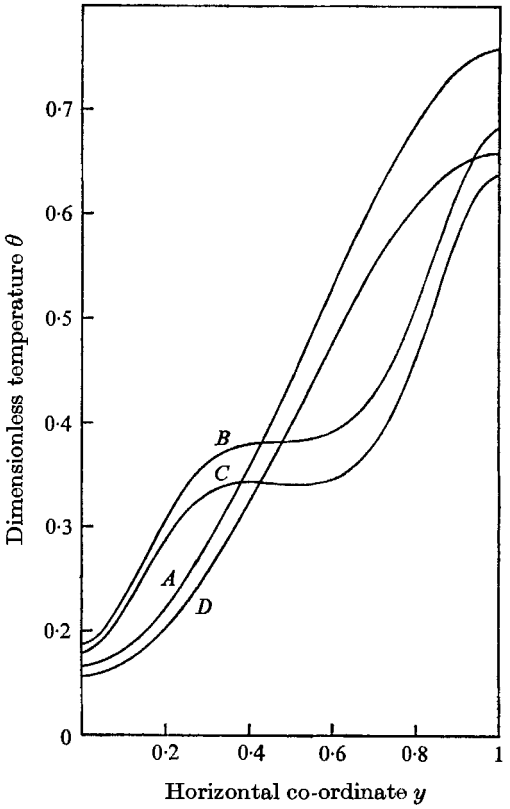

FIGURE 9. The distribution of temperature across the mid-height of the layer for cases *A–D*.

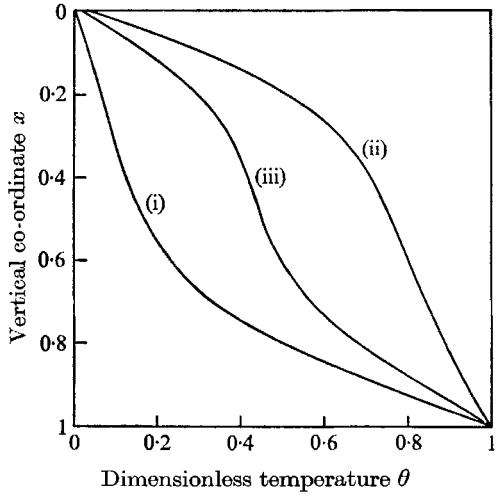

FIGURE 10. The vertical temperature distribution for case *A* for (i) the downward current, (ii) the upward current, and (iii) the horizontally averaged temperature.

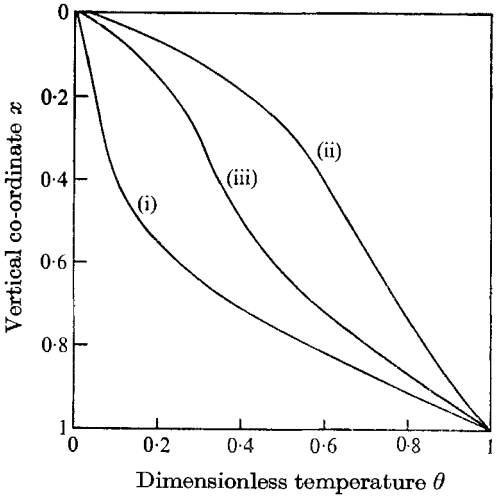

FIGURE 11. The vertical temperature distribution for case *D* for (i) the downward current, (ii) the upward current, and (iii) the horizontally averaged temperature.

the Malkus theory. However, in view of the work of Schlüter *et al.*, we see no reason to discard his criterion.

Figure 13 displays the effect of Gr and Ma on the optimum aspect ratio α. It is seen that α decreases with increasing Ma and also (except at low Gr and high Ma) with increasing Gr. Experimental evidence supporting this behaviour was provided by Koshmieder (1967). However, the opposite effect was observed

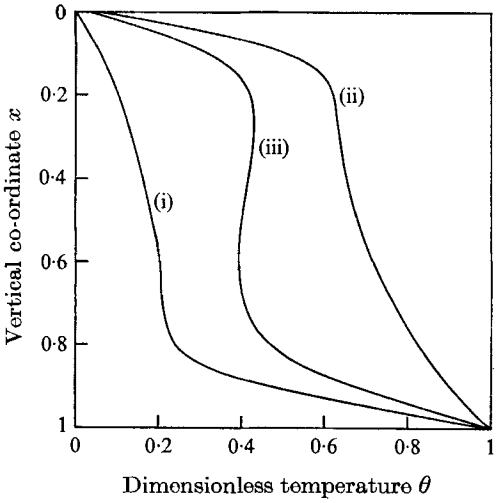

FIGURE 12. The vertical temperature distribution for case C for (i) the downward current, (ii) the upward current, and (iii) the horizontally averaged temperature.

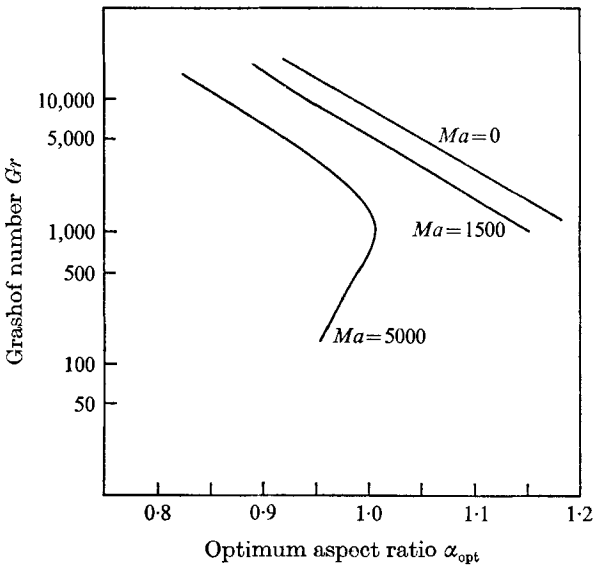

FIGURE 13. The variation of the optimum aspect ratio with the Grashof and Marangoni numbers at $Pr = 1$ and $Bi = 100$.

also by Koshmieder (1966), in the case of convection in fluids contained between two rigid horizontal surfaces. From an analytical study, Schlüter *et al.* have shown that, for layers of infinite extent, the optimum wavelength would indeed decrease with increasing (super-critical) Grashof number, while Davis (1968), using the same assumption of maximization of heat transfer, showed that the influence of rigid *side* walls was to cause the reverse effect to occur.

In the search for the aspect ratio which maximizes the Nusselt number, it soon became obvious that initial conditions played an important role, not only in the development of the flow, but also frequently in the final mode of motion.

The following examples illustrate, first, the effect of a sudden change in one of the parameters (Ma), and secondly, the effect of gradually increasing the aspect ratio.

A converged solution was obtained for $Gr = 10^3$, $Ma = 10^4$, $Bi = 10^2$, $Pr = 3{\cdot}8$, the optimum aspect ratio being 0·91 and the solution consisting of one roll. This, when used as starting data for a higher Marangoni number of $2{\cdot}10^4$ and an aspect ratio of 0·50 (the other parameters remaining constant), produced a two-roll solution, indicating instability of the one-roll solution to large perturbations

(here a sudden change in Marangoni number). This effect was also found to be dependent on the magnitude of the Biot number, and it is reviewed later.

A further reduction of the aspect ratio to 0·40 (using the two-roll solution as starting data) led to a one-roll solution. The original (one-roll) starting data was then used to solve the same problem, but the aspect ratio was reduced directly to 0·40. A one-roll solution resulted, identical to that obtained previously. In the search for the maximum Nusselt number, the aspect ratio was then increased gradually and exceeded the original 0·50 (still with a one-roll solution). The optimum α was ultimately found to be 0·57.

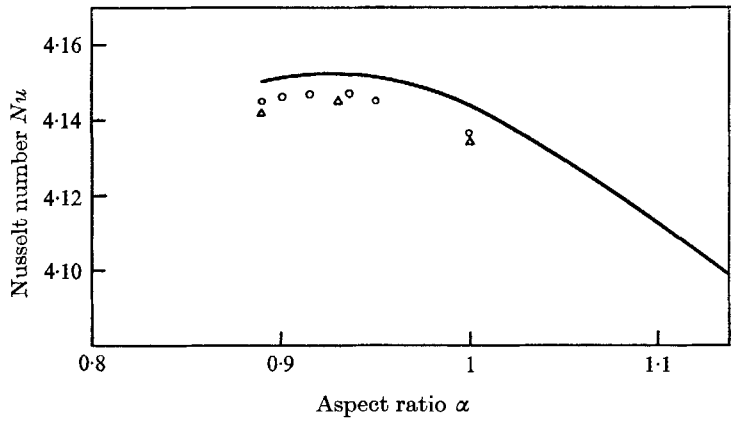

FIGURE 14. The variation of Nusselt number with the aspect ratio at $Gr = 20{,}000$, $Pr = 1$, $Bi = 100$, $Ma = 0$. ——, one-roll solution; △, two-roll solution; ○, three-roll solution.

The second set of numerical experiments compares solutions obtained by gradually increasing the aspect ratio with those obtained when starting directly from rest with a small random temperature perturbation.

For the same aspect ratios, one-, two- and three-roll solutions were obtained. Adjacent rolls of multi-roll solutions were always of opposite rotation, and were obtained by starting with the fluid initially at rest. To ensure comparable accuracy in each case, 21 mesh points were used in the vertical direction, while 21, 41 or 61 points were used in the horizontal direction for the one-, two- and three-roll solutions respectively. The curve of figure 14 was obtained by gradually increasing the aspect ratio of a one-roll solution, while the triangles and circles show respectively the results for two- and three-roll solutions. The one-roll solution was stable to changes in aspect ratio for values of the latter considerably higher than would be obtained when starting from rest. This range of one-roll stability, however, was found to decrease with increasing Marangoni number.

Note that the Nusselt number scale exaggerates the differences between the values of Nu for the one-, two- and three-roll solutions. These differences are of the order of 0·2 % and are certainly numerical in origin.

Properties evaluated at surface temperature: effects of Biot number

Because the surface temperature is not constant, and is not known in advance, it is an inconvenient property to use in the specification of the various parameters of the flow. Moreover, with heat transfer at the surface described by a heat transfer coefficient, an additional parameter (the Biot number) is introduced which is, so to speak, external to the main problem and independent of it (although the solution of the problem is not independent of the Biot number).

Once a solution has been obtained, however, it is a simple matter to determine the average surface temperature, which can then be used to calculate values of Gr, Ma and Nu which apply just to the liquid layer. Denoting the dimensionless average surface temperature by θ_{sa}, it can readily be shown that these 'layer parameters', when based on the difference between the lower surface temperature and θ_{sa}, are given by

$$Gr_s = (1-\theta_{sa})\,Gr, \quad Ma_s = (1-\theta_{sa})\,Ma, \quad Nu_s = Nu/(1-\theta_{sa}).$$

Clearly, as Bi increases, θ_{sa} approaches zero; this causes the layer parameters to approach more closely the overall values. Furthermore, the extent to which the surface temperature can vary is thereby limited, and hence Marangoni number effects are diminished.

An indication of the influence of the Biot number on the layer and overall parameters is provided in table 2.

Case	Bi	Pr	Gr	Ma	Nu	Gr_s	Ma_s	Nu_s
E	100	1	20,000	0	4·152	19,173	0	4·331
F	1	1	20,000	0	0·770	4,855	0	3·172
G	100	1	6,000	5,000	3·370	5,800	4,893	3·486
H	1	1	30,000	5,000	0·793	5,930	988	4·013

TABLE 2. Effect of the Biot number on the effective parameters

For $Bi = 100$ and $Bi = 1$, and for identical Gr and Ma (overall values), the tabulated results for cases E and F show the layer Grashof numbers to be in the ratio of approximately 4:1. The overall Nusselt number is also seen to be strongly affected, while Nu_s shows some decrease which is in accord with the reduced Gr_s. For cases G and H, while the overall values of Gr are in a ratio of 1:5, the layer values of this parameter are in much closer proximity. (It is practically impossible to predict overall values which, for different Bi, will yield identical layer parameters.) Under these conditions, the resulting layer Marangoni numbers are in the ratio of approximately 5:1, and Nu_s has increased. It was generally found that, for approximately equal layer parameters, Nu_s increased with decreases in Bi.

The Biot number also had an influence on the preferred wavelength. In the absence of surface tension effects, the optimum value of α increased with increasing Bi. As Ma was increased, however, this effect became less pronounced, and was even reversed for large enough values of the Marangoni number, as shown in table 3.

It was generally found that the surface tension effects (shift of roll centre, value of α_{opt}, etc.) were more pronounced for a smaller Biot number. This could reasonably be expected, since a higher thermal resistance allows a greater variation in temperature at the free surface, and therefore greater variation in net surface tension force.

Gr_s	Ma_s	α_{opt} at $Bi = 100$	α_{opt} at $Bi = 1$
1654	0	1·15	1·24
3226	0	1·09	1·18
6715	0	1·03	1·13
5930	988	1·01	1·03
3889	1945	1·02	1·02
1085	2171	1·12	1·02

TABLE 3. Effect of the Biot number on the preferred wavelength

As already mentioned, $Bi = 100$ is not really a practical value. It has been established, however, that the solutions obtained with that value are representative of what can be expected from more realistic values. The use of a large Bi was convenient from a computational viewpoint as it simplified and shortened the search for the optimum aspect ratio. This follows from the greater sensitivity of the pattern of the solution to large changes in Ma at small values of Bi, compared with the sensitivity at large Bi.

For example, at $Bi = 100$, a one-roll solution experiencing a change in Ma of 5000 would generally remain a one-roll solution; at $Bi = 1$, however, the same change in Ma would be too drastic and would cause a two-roll solution to form unless there was a corresponding (and sufficient) reduction in α. Since α was not known, this situation was difficult to avoid. An alternative procedure would have been to start each solution from rest, and in view of the difficulties encountered, this might well have been a better approach!

Prandtl number effects

Many of the results were obtained with a Prandtl number of unity. This value was not chosen for any special reason; the aim was to obtain results and study effects rather than to simulate any particular fluid.

Some results were, however, obtained with higher Prandtl numbers. These showed that, in common with other buoyancy-driven flows, the characteristics of the Bénard cell are generally more conveniently described in terms of the Rayleigh number $Ra = Gr.Pr$, rather than Grashof number, or, better still, in terms of the layer Rayleigh number $Ra_s = Ra(1 - \theta_{sa})$. It was found that Pr had little effect on either the general features of the flow pattern or on the optimum mode of motion. Nevertheless, the dimensionless parameters describing the flow field were affected as shown in figures 15–17, and the Nusselt number decreased somewhat with an increase in Prandtl number (for a constant Rayleigh number) as shown in table 4.

The value of the Prandtl number generally affected the velocity distribution in the liquid. At a Prandtl number of unity, the downward current had a higher velocity than the upward current. However, as the value of Pr was increased, this condition was not necessarily maintained (particularly when surface tension

Gr	Ma	Pr	Ra_s	Nu	Nu_s
18,000	0	1	17,279	4·6410	4·8343
9,000	0	2	17,291	4·5923	4·7807
4,500	0	4	17,303	4·5020	4·6833

TABLE 4. Effect of Prandtl number on Nusselt number

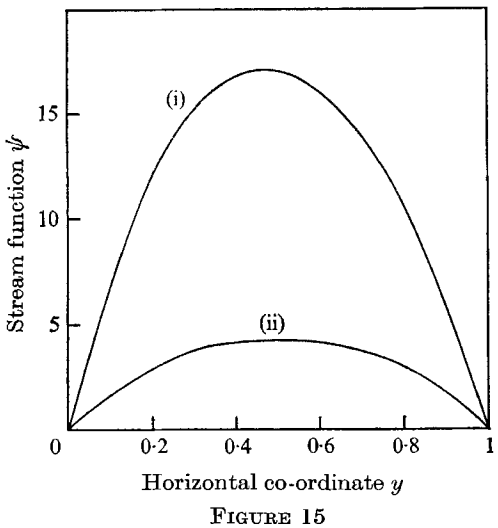

FIGURE 15

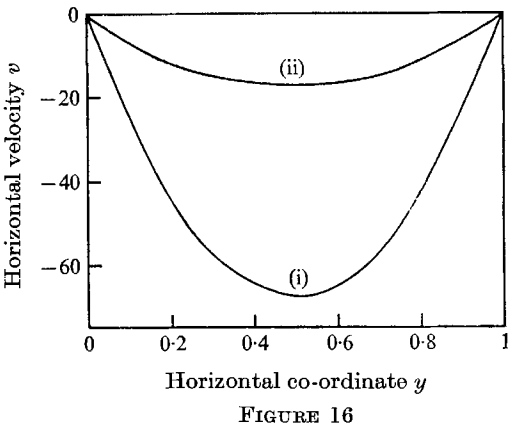

FIGURE 16

FIGURE 15. The effect of Prandtl number on the distribution of stream function across the mid-height of the layer for (i) $Gr = 18{,}000$, $Pr = 1$, $Bi = 100$, $Ma = 0$ and (ii) $Gr = 4500$, $Pr = 4$, $Bi = 100$, $Ma = 0$.

FIGURE 16. The effect of Prandtl number on the distribution of horizontal velocity across the surface of the layer for (i) $Gr = 18{,}000$, $Pr = 1$, $Bi = 100$, $Ma = 0$ and (ii) $Gr = 4500$, $Pr = 4$, $Bi = 100$, $Ma = 0$.

effects were absent). For instance, at $Pr = 3{\cdot}8$, $Gr = 1750$, $Bi = 100$, $Ma = 0$, the upward current had a higher velocity over the lower half of the roll and the absolute maximum vertical velocity occurred in the ascending fluid. As the Marangoni number was increased to 5000, however, the region over which the absolute upward velocity exceeded the downward velocity was decreased and the absolute maximum vertical velocity was found again to occur in the descending fluid. This surface tension effect is easy to understand, since the descending fluid has been further accelerated at the free surface, whereas the ascending fluid is retarded by the rigid lower surface. As a further result, the position of the maximum vertical velocity has moved upwards.

The work of Samuels (1966), describing the motion of fluids enclosed between rigid boundaries and uniformly heated at the lower surface, showed that the

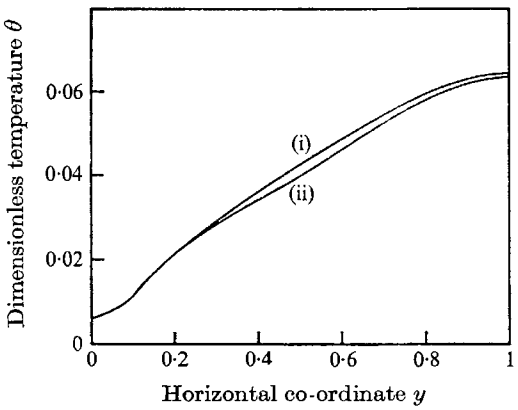

FIGURE 17. The effect of Prandtl number on the distribution of temperature across the surface of the layer for (i) $Gr = 18{,}000$, $Pr = 1$, $Bi = 100$, $Ma = 0$ and (ii) $Gr = 4500$, $Pr = 4$, $Bi = 100$, $Ma = 0$.

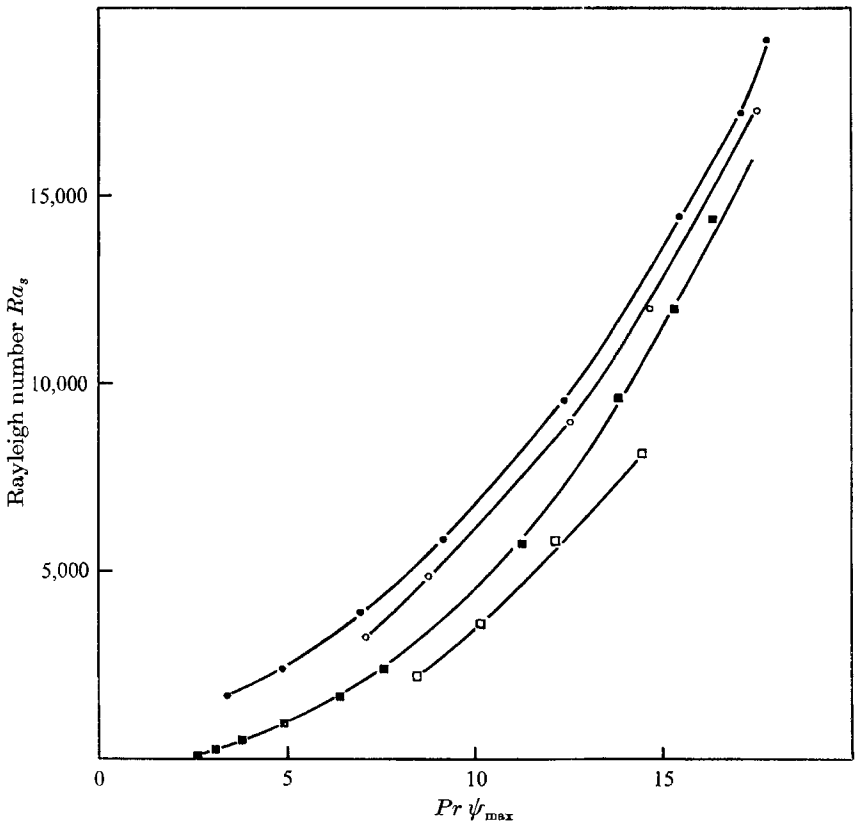

FIGURE 18. The dependence of $Pr\psi_{max}$ on the fluid flow parameters: ●, $Ma = 0$, $Bi = 100$, $1 < Pr < 20$; ○, $Ma = 0$, $Bi = 1$, $1 < Pr < 20$; ■, $Ma = 5000$, $Bi = 100$, $Pr = 1$; □, $Ma = 5000$, $Bi = 100$, $Pr = 3{\cdot}8$. (For the sake of clarity not all the computed points are shown.)

dimensionless quantity $Pr\,\psi_{\max}$ was a function of Ra only, when the Prandtl number exceeded a value of unity. With a free upper surface, and considering the effect of surface tension, we have two additional parameters to contend with, namely the Biot and Marangoni numbers. It was found that for stress-free surfaces, for a fixed Biot number and for Pr in the range 1–20, $Pr\,\psi_{\max}$ was indeed a function of Ra_s only, as shown in figure 18. However, $Pr\,\psi_{\max}$ was found to be a function of Bi. Furthermore, once surface tension effects were introduced, it was found that the relationship was no longer independent of the Prandtl number, and an increase of the latter caused an increase in $Pr\,\psi_{\max}$.

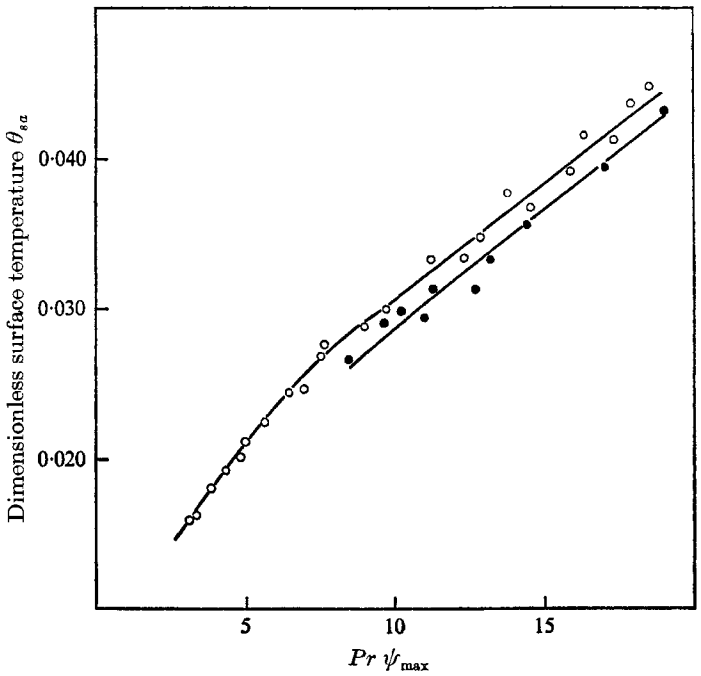

FIGURE 19. The dependence of the horizontally averaged surface temperature on $Pr\,\psi_{\max}$ at a Biot number of 100 for (○) $Pr = 1$ and (●) $Pr = 3{\cdot}8$. For the sake of clarity not all the computed points are shown. Both curves were obtained for a range of Ra of 1,000–20,000 and a range of Ma of 0–10,000.

We may think of $Pr\,\psi_{\max}$ as a measure of the strength of convection, and, intuitively, we would expect an increase in mean free surface temperature to be associated with stronger motion. This was in fact always the case, and figure 19 shows that the relationship between the mean upper surface temperature and the strength of convection was independent of the nature of the motion (i.e. purely convective, surface tension driven, or any combination of the two). It is obvious that such relationship could only hold for a particular value of the Biot number. The results shown in figure 19 were obtained from solutions with a Biot number of 100 and for a range of Gr and Ma. As the Prandtl number increased, for the same strength of convection, the surface temperature was generally found to decrease.

Heat transfer

The heat transfer across the cavity was separated into convective and conductive modes, and the typical results of figures 20 and 21 again show that for higher Grashof numbers we obtained regions of negative conduction. This effect was not observed experimentally by either Somerscales & Dropkin (1966) or Di Federico & Foraboshi (1966) in the turbulent régime of convection, but a similar effect was observed by Elder (1965) and MacGregor & Emery (1968) for laminar convection between vertical plates. As the strength of convection increased, the upper and lower convection layers became thinner and the central region of high convective contribution increased in size.

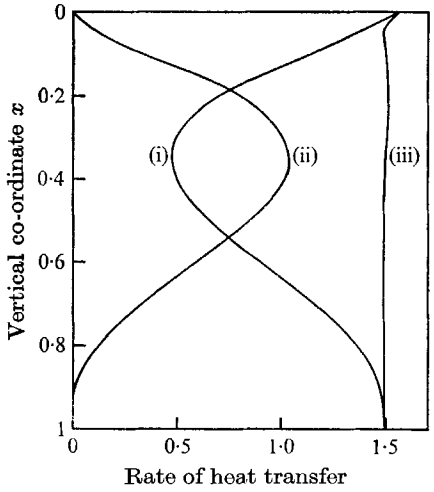

FIGURE 20. The rate of heat transfer through the layer for case D (i) by conduction, (ii) by convection and (iii) total.

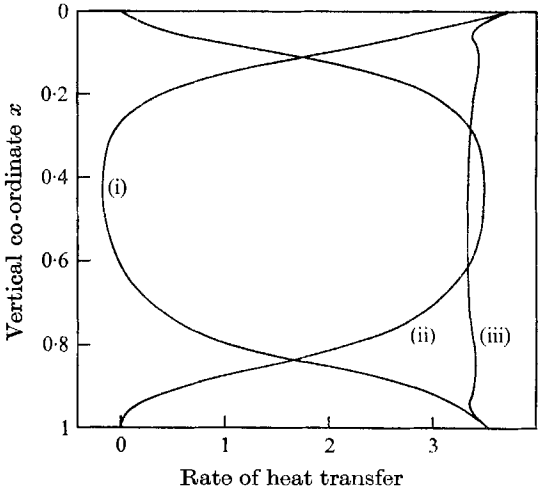

FIGURE 21. The rate of heat transfer through the layer for case B (i) by conduction, (ii) by convection and (iii) total.

The addition of the two effects should give constant total heat transfer across the cavity, since the side boundaries are adiabatic. However, the use of a one-sided finite difference approximation at the horizontal boundaries as against central differences throughout the rest of the domain gave results consistently higher at the boundaries. This effect was more pronounced at higher Gr and Ma, when higher velocities may be expected. As a result, it was felt that the best estimate of the heat transfer rate was provided by the values of Nu at the mid-height of the liquid layer.

Heat transfer results at the optimum wavelength for surface Rayleigh numbers ranging up to 20,000, and Marangoni numbers of 0, 1500 and 5000 were obtained at a Biot number of 100 and a Prandtl number of 1. They are shown on figure 22, which indicates a form of relationship similar to that obtained experimentally. Since the effective Marangoni number is not known *a priori*, and also since it varies for different solutions (except in the case of $Ma = 0$), it is almost impossible to obtain results which, for a range of effective Rayleigh numbers, will have

identical values of Ma_s. The curves are therefore shown as a function of the overall Marangoni number. At $Ma = 5000$, for instance, the value of Ma_s varied from 4775 at $Ra = 20\,000$ to 4926 at $Ra = 100$. (From the results of figures 18 and 19 it is obvious that for increasing Ra_s, the surface temperature increases and hence the effective value of Ma decreases.)

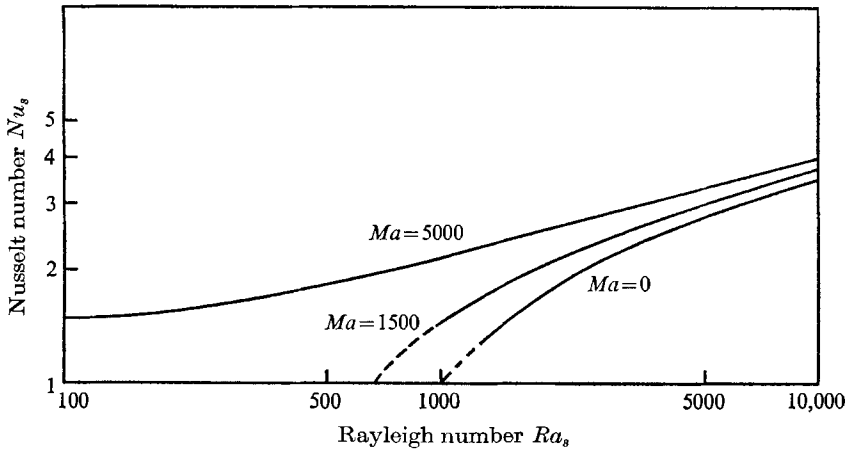

FIGURE 22. The variation of the Nusselt number as a function of Rayleigh number at $Pr = 1$ and $Bi = 100$.

Stability

It is well established that for buoyancy driven convection, there exists a critical Rayleigh number below which any disturbance imparted to the fluid will decay. Nield (1964) has shown that when the effects of surface tension are added to the effects of buoyancy, there also exists a critical Marangoni number, and that certain combinations of Ma and Ra must be exceeded before motion impends. The form of the relationship between Ma and Ra is a weak function of the Biot number.

It was difficult, in a reasonable amount of computer time, to determine the stability limits with any precision, even when the effect of only a limited number of parameters (Ra and Ma) was studied. The method used was to disturb randomly (usually through the temperature field) an initially stationary fluid, and observe whether the ensuing motion decayed to rest again or reached a steady non-zero value (of stream function). For each case this would take an appreciable amount of computer time (of the order of 10 to 15 min). The domain was taken to have an aspect ratio of unity, and, bearing in mind that the optimum also had to be determined, it will be realized that the location of the stability limit by this method is not particularly efficient. It, nevertheless, yielded some results which, within the limits of the accuracy used (large steps in Ra and Ma) agreed surprisingly well with those of Nield.

A typical set of transients for the maximum value of the stream function is shown in figure 23; from these results, the stability limit was taken to lie in the

range of Grashof numbers between 800 and 900. From a succession of such results, we derived the marginal stability curve shown in figure 24, which was obtained for $Bi = 100$ and $Pr = 1$.

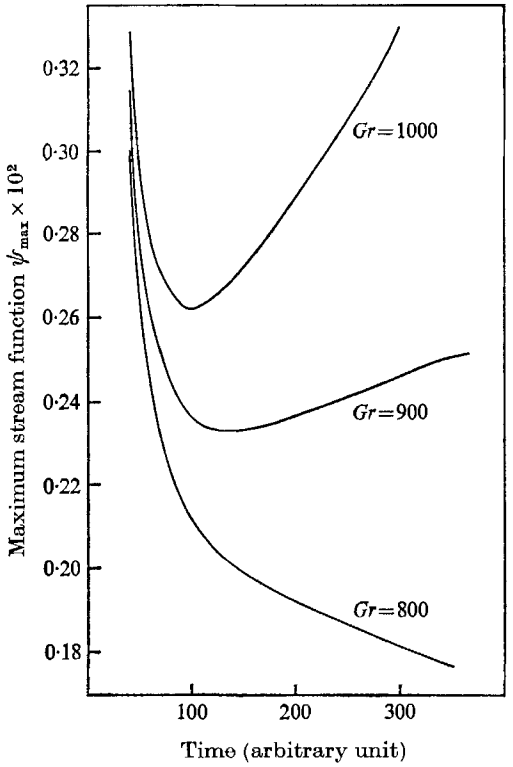

FIGURE 23. Typical transients of the maximum value of stream function for $Ma = 1000$, $Pr = 1$, $Bi = 100$.

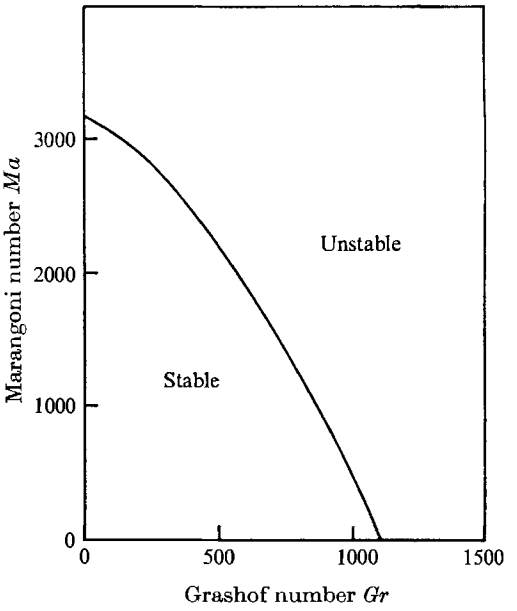

FIGURE 24. Critical stability curve for $Bi = 100$, $Pr = 1$.

Another approach to the critical parameters is the extrapolation of the heat transfer relationship to a Nusselt number of unity (based on the mean free surface temperature). From figure 22 it is obvious that, while a critical Rayleigh number exists for $Ma = 0$ and $Ma = 1500$, it will not be found for $Ma = 5000$ (i.e. a Marangoni number of 5000 is supercritical at all Rayleigh numbers).

The critical parameters obtained by these two methods may be compared with Nield's results. At $Ma = 0$, we find $Ra_c = 1100$ from our marginal stability curve, and $Ra_c = 1000$ from the extrapolated heat transfer relationship of figure 22. The value given by Nield was 1086. For $Ra = 0$ in figure 24, we find $Ma_c = 3200$, while Nield gives a value of 3304. It can easily be shown that at critical stability, the surface temperature is given by $1/(1+Bi)$ and that the effective Marangoni number is therefore equal to $Ma.Bi/(1+Bi)$. At $Ma = 1500$, our effective critical parameters were $Ma_c = 1485$, $Ra_c = 650$. From figure 1

and table 1 of Nield's paper, the critical Rayleigh number for $Bi = 100$, $Ma = 1485$ is found to be approximately 685. The agreement in all these comparisons is very satisfactory.

Periodic or symmetric boundary conditions

Experimental evidence (Berg *et al.* 1966) is sufficient to justify the belief that, under appropriate conditions, a liquid which is heated from below will form itself into a series of two-dimensional rolls. There is no doubt, therefore, that it is valid to seek solutions to the governing equations by imposing conditions of periodicity on the stream function, vorticity and temperature. It now remains to examine whether, as one would tend to suspect, the periodicity extends to adjacent rolls (with the necessary sign changes) or only to adjacent roll pairs. Since the consequent saving in both computer time and storage requirements made the use of symmetric boundary conditions most appealing, it was felt necessary to devote some effort to justifying their validity.

If the motion in adjacent rolls is symmetric, it may be concluded that the streamline dividing them is vertical, and that the horizontal temperature gradient, the horizontal velocity component and the vorticity along this line are all zero. Solutions obtained with the use of periodic boundary conditions were therefore examined to test this conclusion, and were also compared with solutions obtained using the same parameters and symmetric boundary conditions.

Table 5 records the co-ordinates of the lines $\psi = 0$ on either side of anticlockwise rolls computed using periodic boundary conditions with several sets of solution parameters, and also the horizontal temperature gradients along these lines. For convenience, the aspect ratio used was unity, and variations in the horizontal co-ordinate with depth therefore give the departure (in fractions of the roll width) of the dividing streamline from the vertical.

It can be seen that the deviation from the vertical is largest at the highest value of Ma and the lower value of Bi, i.e. when surface tension effects are at their strongest. It should be kept in mind, however, that this maximum deviation of 0·02061 is only about two-fifths of one mesh length or about 2 % of the roll width. For this case, the horizontal temperature gradients along the dividing streamlines are seen to be very small (about 3 % of the maximum internal value of 0·0572). In other examples, both the deviations from the vertical, and the boundary horizontal temperature gradients, are very much smaller.

Table 6 compares some descriptors of the motion found with the two boundary conditions. It can be seen that at zero or low Ma the differences are negligible. As Ma was increased, the situation deteriorated somewhat.

It is not unreasonable to suggest that these experiments validate the belief that the motion in adjacent rolls is symmetric. Although there is a progressive departure from this condition as, in particular, Ma increases, it is plausible that this is not a true feature of the flow, but an indication of increasing truncation errors associated with the finite difference approximations used. In either case, we felt justified in the belief that the use of the symmetric boundary condition would not introduce appreciable errors.

Gr	6,000		6,000		20,000	
Ma	0		9,000		10,000	
Pr	1		1		3·68	
Bi	100		100		0·1	
Vertical co-ordinates	Left	Right	Left	Right	Left	Right
0·0	0·00125	1·00081	0·00074	1·00875	0·00104	1·00195
0·1	0·00125	1·00081	0·00127	1·00679	0·00314	1·00550
0·2	0·00126	1·00082	0·00190	1·00563	0·00545	1·00855
0·4	0·00127	1·00080	0·00230	1·00463	0·01000	1·01330
0·6	0·00125	1·00080	0·00192	1·00390	0·01350	1·01705
0·8	0·00125	1·00084	0·00150	1·00320	0·01710	1·01995
0·9	0·00124	1·00101	0·00160	1·00287	0·02165	1·02120
Max. departure from vertical	0·00003	0·00020	0·00156	0·00588	0·02061	0·01925

(*a*)

0·0	0·0005	−0·0005	0·0014	0·0012	0·0010	0·0007
0·1	0·0006	−0·0006	0·0027	0·0056	0·0016	0·0009
0·2	0·0010	−0·0009	0·0085	0·0053	0·0014	0·0009
0·4	0·0008	−0·0016	0·0145	0·0000	0·0019	0·0011
0·6	0·0004	−0·0024	0 0106	0·0000	0·0006	0·0011
0 8	0·0008	−0·0008	0·0068	−0·0008	0·0003	0·0007
0 9	0·0010	−0·0003	0·0086	−0·0010	0·0002	0·0003
Max. horiz. temperature gradient	1·1375		1·3535		0·0572	

(*b*)

TABLE 5. (*a*) Horizontal co-ordinates at $\psi = 0$. (*b*) Horizontal temperature gradient along $\psi = 0$. *Note*: The horizontal co-ordinates of the line $\psi = 0$ at the lower boundary could only be determined approximately by locating the position of the maximum and minimum values of the vertical temperature gradient. These co-ordinates have therefore not been included in the table

	$Gr = 6 \times 10^3, Pr = 1, Ma = 0, Bi = 10^2$				$Gr = 6 \times 10^3, Pr = 1, Ma = 5 \times 10^3 Bi = 10^2$			
	Periodic		Symmetric		Periodic		Symmetric	
	Min	Max	Min	Max	Min	Max	Min	Max
Stream function	0	8·9	0	8·9	0	11·0	0	11·2
Vertical velocity	−29·4	33·1	−29·5	33·2	36·2	52·3	−36·8	54·6
Horizontal velocity	−33·1	25·6	−33·1	25·6	−59·8	31·1	−61·3	31·6
Vorticity	−305·7	170·4	−305·7	175·3	−396·1	519·3	−405·9	541·8
Nusselt number	3·0766		3·0766		3·7184		3·7754	

TABLE 6. Comparison of results for period and symmetric boundary conditions

Conclusion

This is the first time, to the authors' knowledge, that surface tension effects have been incorporated into the full solution of the equations of mass, momentum and energy conservation. As was predicted by linear theory (and confirmed by

experiments) these effects encourage the motion when surface tension is a decreasing function of temperature (as it is for all known liquids). Whilst a full parametric study of this problem does not seem possible within a reasonable amount of computer time, many of the general properties of the flow have been obtained. The effects of flow parameters (*Ra*, *Pr*, *Bi*, *Ma*) on the preferred mode of motion were also studied subject to the Malkus criterion of maximum heat transfer. As a result of numerical experiments, it was found that the condition of symmetry on adjacent rolls was quite acceptable while having the obvious advantage of reducing the solution time considerably.

This work was supported by the Australian Research Grants Committee, for which the authors are grateful.

REFERENCES

BÉNARD, H. 1900*a* *Rev. Gen. Sci. Pures Appl. Bull. Assoc. Franc. Avanc. Sci.* **11**, 1261.
BÉNARD, H. 1900*b* *Rev. Gen. Sci. Pures Appl. Bull. Assoc. Franc. Avanc. Sci.* **11**, 1309.
BERG, J. C., ACRIVOS, A. & BOUDART, M. 1966 *Adv. Chem. Engng*, **6**, 61.
BRIAN, P. L. T. 1961 *A.I.Ch.E. J.* **7**, 367.
DAVIS, S. H. 1968 *J. Fluid Mech.* **32**, 619.
DI FEDERICO, I. & FORABOSHI, F. P. 1966 *Int. J. Heat Mass Transfer*, **9**, 1351.
ELDER, J. W. 1965 *J. Fluid Mech.* **23**, 77.
FOSTER, T. D. 1969 *J. Fluid Mech.* **37**, 81.
GREENSPAN, D. 1968 *Computer Science Tech. Rep.* 37. University of Wisconsin.
KOSCHMIEDER, E. L. 1966 *Beitr. Phys. Atmos.* **39**, 1.
KOSCHMIEDER, E. L. 1967 *J. Fluid Mech.* **30**, 9.
MACGREGOR, R. K. & EMERY, A. F. 1969 *Trans. ASME* (*C*), *J. Heat Transfer*, **3**, 391.
MALKUS, W. V. R. 1954*a* *Proc. Roy. Soc.* A **255**, 185.
MALKUS, W. V. R. 1954*b* *Proc. Roy. Soc.* A **225**, 196.
NIELD, D. A. 1964 *J. Fluid Mech.* **19**, 341.
PEARSON, J. R. A. 1958 *J. Fluid Mech.* **4**, 489.
PILLOW, A. F. 1952 *Aust. Dept. Supply Aero. Res. Lab. Rep.* A 79.
ROBINSON, J. L. 1967 *J. Fluid Mech.* **30**, 577.
SAMUELS, M. R. 1966 Ph.D. Thesis, University of Michigan.
SCHULTER, A., LORTZ, D. & BUSSE, F. 1965 *J. Fluid Mech.* **23**, 129.
SCRIVEN, L. & STERNLING, C. 1964 *J. Fluid Mech.* **19**, 321.
SMITH, E. A. 1966 *J. Fluid Mech.* **24**, 401.
SOMERSCALES, E. F. C. & DROPKIN, D. 1966 *Int. J. Heat Mass Transfer*, **9**, 1189.
THOMPSON, J. J. 1855 *Phil. Mag.* (4) **10**, 330.